DECOUPLED DISTURBANCE OBSERVERS FOR DUAL-INPUT-SINGLE-OUTPUT SYSTEMS WITH APPLICATION TO VIBRATION REJECTION IN DUAL-STAGE HARD DISK DRIVES

Xu Chen
Department of Mechanical Engineering
University of California, Berkeley
Berkeley, California 94720
Email: maxchen@me.berkeley.edu

Masayoshi Tomizuka
Department of Mechanical Engineering
University of California, Berkeley
Berkeley, California 94720
Email: tomizuka@me.berkeley.edu

ABSTRACT

The disturbance observer (DOB) has been one effective robust control approach for servo enhancement in single-input-single-output systems. This paper presents a new extension of the DOB idea to dual-input-single-output systems, and discusses an optimal Q-filter design. The proposed decoupled disturbance observer (DDOB) provides a flexible approach to use the most suitable actuators for compensating disturbances at different frequencies. Such a scheme is helpful, e.g., for modern dual-stage hard disk drives, where enhanced servo design is becoming more and more essential in the presence of audio vibrations.

1 INTRODUCTION

With the ever increasing demand of larger capacity in hard disk drive (HDD) systems, dual-stage actuation has become an essential technique to break the bottleneck of the servo performance in single-actuator HDDs [1, 2]. In this structural configuration, the microactuator has enhanced mechanical performance in the high-frequency region, providing the capacity to greatly increase the servo bandwidth. Among different choices of the secondary actuators, piezoelectric (PZT) microactuators have various creditable properties and have been the research focus since their appearance (see, e.g., [3, 4] and the references therein). In this dual-input-single-output (DISO) system, the two actuators receive respectively current and voltage inputs, while only the position error of the read/write head is measurable for servo control.

Despite the mechanical advantages, compared to single-stage HDDs, much less research has been conducted to the servo control of a dual-stage HDD. One algorithm that is useful for single-stage HDDs [5, 6] but not well developed for dual-stage HDDs, is the disturbance observer (DOB) [7]. The DOB counteracts the disturbance by its estimate, which is generated by utilizing an inverse model of the plant and a so-called Q filter. As a flexible and powerful add-on element for servo enhancement, DOB has had broad applications in fields other than HDDs, including but not limited to: optical disk drives [8], linear motors [9], positioning tables [10], robot arms [11], and automotive engines [12]. These results are also restricted to single-input-single-output (SISO) systems, while the generalization to DISO plants has not been fully addressed. Among the related literature, [13] applied one conventional DOB to each actuator in a dual-stage HDD. The final position of the DISO system here is the summation of the outputs of the two actuators: Voice-Coil-Motor (VCM) actuator and Microactuator. The conventional DOB for the *microactuator* treated the first-stage output and the actual disturbance as an effective total disturbance, and tried to cancel it. In the mean time, for the *VCM actuator*, the actual disturbance was also regarded (together with the microactuator output) as part of the effective disturbance in the VCM DOB. What is unclear here is that what portion of the actual disturbance is canceled by each DOB. If the cancellation of the low-frequency components relied too heavily on the microactuator, a complicated consequence may arise since the moving range of the microactuator is very limited. Safety concerns will also arise as DOB for the microactuator treated the first-stage output as an internal disturbance,

and tended to undo the achieved (long-range) movement of the VCM actuator. References [14] and [15] discussed state-space designs to implement the idea of disturbance observers in special classes of MIMO systems. Within this framework, the transfer-function approach of model inversion and Q-filter design was replaced with an observer-type state-space construction. A customized treatment of DISO systems was not given. Independent application of each actuator for disturbance rejection (decoupled disturbance compensation) was not achieved.

Two main limitations in the generalization of DOB to DISO system have been the nontrivial model inversion and the distribution of the compensation efforts. This paper proposes a new decoupled disturbance observer (DDOB) to simplify the above obstacles. Different from previous literature, the coupling of individual channels is directly considered in the structural DDOB design, resulting in several advantageous properties. First, a full separation of the actual external disturbances can be achieved. No cross-channel coupling effects enter as internal disturbances. Second, the proposed scheme has clear time- and frequency-domain design intuitions, which were lacking in [13–15]. Finally, we have the design flexibility to distribute the compensation effort according to the mechanical properties of each actuator and the frequency range of the disturbances. These features make DDOB beneficial for the compensation of audio vibrations in HDDs. This type of problem is faced more and more in modern HDDs, as high-power speakers in multimedia applications (such as all-in-one computers and digital TVs) generate large amounts of external disturbances. Such vibrations are extremely difficult to handle in a cost-effective way for HDDs, due to their intrinsic properties of (a) environmental dependence; (b) appearing in a wide frequency range (from 300 Hz to as high as 4 kHz); and (c) having multiple resonances and wide spectral peaks [16].

In the remainder of the paper, we will discuss the design of DDOB for general DISO systems. The practical implementation on HDDs will be incorporated as a design example throughout the discussion. Sections 2 and 3 provide respectively the controller structure and the stability conditions. The central design of the Q filter is shown in Section 4 (the proposed optimal Q-filter construction is also suitable for SISO DOBs). Section 5 provides a detailed case study. Section 6 concludes the paper.

2 DDOB STRUCTURE

We start by considering a general discrete-time linear time-invariant DISO system $P(z^{-1}) = [P_1(z^{-1}),\, P_2(z^{-1})]$, with the input-output relation:

$$y(k) = P_1(z^{-1})u_1(k) + P_2(z^{-1})u_2(k) + d(k). \tag{1}$$

Here $y(k)$, $u_i(k)$ $(i = 1,2)$ and $d(k)$ represent respectively the plant output, the plant inputs, and the lumped external disturbance. We will slightly abuse the notation $P_i(z^{-1})$ to denote a transfer function and pulse transfer function, so that $P_i(z^{-1})u_i(k)$ represents the time-domain output of $P_i(z^{-1})$. Fig. 1 shows the structure of the proposed DDOB for the second channel $P_2(z^{-1})$. The idea is to apply the compensation signal $c_2(k)$ to one actuator (in this case the second actuator), such that the overall lumped disturbance $d(k)$ is compensated. Throughout the paper, we denote $\hat{P}_i(z^{-1})$ as the nominal model of $P_i(z^{-1})$ $(i = 1,2)$, and m_i as the relative degree of $\hat{P}_i(z^{-1})$. In this way, although $\hat{P}_2^{-1}(z^{-1})$ may not be realizable/causal, $z^{-m_2}\hat{P}_2^{-1}(z^{-1})$ in Fig. 1 is proper in its minimal realization.

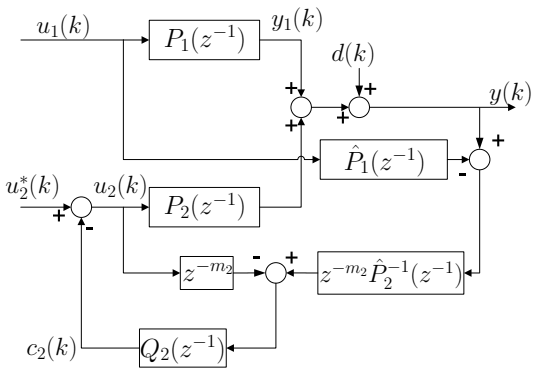

Figure 1: Block diagram of DDOB for $P_2(z^{-1})$.

2.1 Time-domain Disturbance-rejection Criteria

From Fig. 1, the output of $Q_2(z^{-1})$ is given by[1] $c_2 = Q_2[z^{-m_2}\hat{P}_2^{-1}(y - \hat{P}_1u_1) - z^{-m_2}u_2]$. Substituting (1) into this result, we have

$$c_2 = Q_2\Big[z^{-m_2}\hat{P}_2^{-1}(P_1 - \hat{P}_1)u_1 + z^{-m_2}(\hat{P}_2^{-1}P_2 - 1)u_2 + z^{-m_2}\hat{P}_2^{-1}d\Big]. \tag{2}$$

If $P_i(z^{-1}) = \hat{P}_i(z^{-1})$, (2) indicates that

$$c_2(k) = Q_2(z^{-1})z^{-m_2}\hat{P}_2^{-1}(z^{-1})d(k). \tag{3}$$

Notice that $\hat{P}_2^{-1}(z^{-1})d(k)$ can be regarded as an equivalent input disturbance for $P_2(z^{-1})$, and that $c_2(k)$ in (3) is a delayed and filtered version of $\hat{P}_2^{-1}(z^{-1})d(k)$. This "observed" disturbance, after being multiplied by -1 and then added into $u_2(k)$ in Fig. 1, gets filtered through $P_2(z^{-1})$ and

[1] For simplicity, the indexes k and z^{-1} are omitted here.

cancels $d(k)$ ($-P_2c_2(k) \approx -z^{-m_2}Q_2d(k) \approx -d(k)$ if $z^{-m_2}Q_2 \approx 1$), without influencing the output of $P_1(z^{-1})$ (the position output of the first actuator).

2.2 Model-following Property

One can remark that when $P_i(z^{-1})$ differs from $\hat{P}_i(z^{-1})$, the model mismatch is absorbed as an internal disturbance in (2) (see the first two terms in the square brackets). In this subsection we explore this observation in greater details.

Notice that $c_2(k) = u_2(k) - u_2^*(k)$ in Fig. 1. Combining this information with (2), we can solve for $u_2(k)$ and substitute the result to (1), to get: $y(k) = G_{yd}(z^{-1})d(k) + G_{yu_1}(z^{-1})u_1(k) + G_{yu_2^*}(z^{-1})u_2^*(k)$, where the three transfer functions are $G_{yd} = 1 - \frac{\hat{P}_2^{-1}P_2z^{-m_2}Q_2}{1+(\hat{P}_2^{-1}P_2-1)z^{-m_2}Q_2}$, $G_{yu_1} = P_1 - \frac{\hat{P}_2^{-1}P_2(P_1-\hat{P}_1)z^{-m_2}Q_2}{1+(\hat{P}_2^{-1}P_2-1)z^{-m_2}Q_2}$, and $G_{yu_2^*} = \frac{P_2}{1+(\hat{P}_2^{-1}P_2-1)z^{-m_2}Q_2}$.

If $z^{-m_2}Q(z^{-1}) = 1$, we have

$$G_{yd}(z^{-1}) = 0,\ G_{yu_1}(z^{-1}) = \hat{P}_1(z^{-1}),\ G_{yu_2^*}(z^{-1}) = \hat{P}_2(z^{-1}). \quad (4)$$

Here $G_{yd}(z^{-1}) = 0$ explains the disturbance-rejection result in Section 2.1. Additionally, we observe that the dynamics between the nominal inputs (u_1 and u_2^*) and the output now is forced to follow the nominal model $\hat{P}_i(z^{-1})$ ($i = 1, 2$)–thus the rejection of modeling mismatch within the DDOB loop. DDOB hence has the nominal-model-following property. Notice that (4) equally holds if one replaces z^{-1} with $e^{-j\omega}$, in which case the nominal model following is enforced at the frequencies where $e^{-m_2 j\omega}Q(e^{-j\omega}) = 1$.

2.3 Operation of Two DDOBs

Swapping every applicable sub-index between 1 and 2 in the preceding discussions, we get the DDOB for $P_1(z^{-1})$. By linearity and (3), if two DDOBs operate simultaneously, the disturbance compensation is achieved by

$$d(k) - P_1(z^{-1})c_1(k) - P_2(z^{-1})c_2(k) = \left(1 - z^{-m_1}Q_1(z^{-1}) - z^{-m_2}Q_2(z^{-1})\right)d(k). \quad (5)$$

One can remark that if a single DDOB already achieves canceling the disturbance, say, $d(k) - P_1(z^{-1})c_1(k)$ already approximates 0, then the second DDOB is not necessary and we should set $Q_2(z^{-1}) = 0$. This is the ideal situation when one actuator alone can effectively handle all the disturbances. In practice, this may not always be feasible due to the mechanical limitation of the actuators. In addition, notice that $d(k) - P_1(z^{-1})c_1(k) = 1 - z^{-m_1}Q_1(z^{-1})$. It is theoretically not possible for $z^{-m_2}Q(z^{-1}) = 1$ (using a causal $Q(z^{-1})$) to hold over the entire frequency region.[2] The second DDOB can then be used to reduce the residual errors of the first DDOB.

We propose to apply frequency-dependent DDOBs based on the actuator dynamics and disturbance properties. For example, in HDD applications, the VCM actuator ($P_1(z^{-1})$ in Fig. 1) has a large actuation range and the microactuator ($P_2(z^{-1})$ in Fig. 1) suits only for small-range positioning. Additionally, $\hat{P}_1^{-1}(z^{-1})$ has properties similar to a double differentiator in the high-frequency region [5, 6], yielding large high-frequency noises in the output of $\hat{P}_1^{-1}(z^{-1})$. Such actuator dynamics renders VCM DDOB to have increased difficulties as the disturbance frequency gets higher and higher. The microactuator on the other hand has a model of a DC gain plus resonances above 4 kHz, and a better signal-to-noise ratio during implementation of $\hat{P}_2^{-1}(z^{-1})$. From the above considerations, in the low-frequency region, we can apply DDOB to the large-stroke VCM actuator, by assigning $Q_1(z^{-1})$ to be a low-pass/band-pass filter and $Q_2(e^{-j\omega}) \approx 0$. At middle and high frequencies, the precise and faster-response microactuator can be more effectively used. This is achieved by assigning $Q_1(e^{-j\omega}) \approx 0$ and $Q_2(z^{-1})$ to have a band-pass structure. Throughout this paper, unless otherwise stated, we assume the above decoupled disturbance-rejection scheme.

3 STABILITY AND LOOP-SHAPING CRITERIA

This section discusses the design criteria and the closed-loop stability when DDOB is applied to a closed loop consisting of the DISO plant and a baseline feedback controller $C(z^{-1}) = [C_1(z^{-1}), C_2(z^{-1})]^T$. Fig. 2 shows the proposed controller implementation. We will present analysis of DDOB for the secondary actuator. The result for the first actuator is obtained by inter-changing the sub-indexes in the transfer functions.

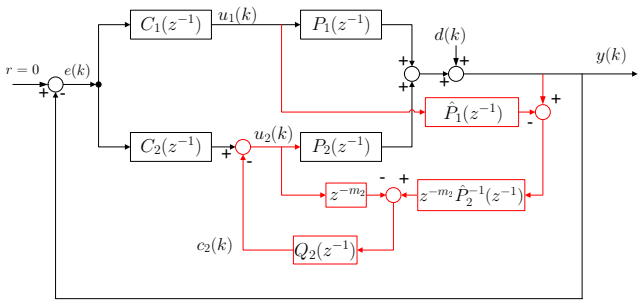

Figure 2: Closed-loop block diagram with DDOB for $P_2(z^{-1})$.

[2] There are also stability constrains when the plant model $\hat{P}_i(z^{-1})$ does not fully capture $P_i(z^{-1})$.

It can be shown (see Appendix A) that the block diagram in Fig. 2 is equivalent to that in Fig. 3, where DDOB affects the secondary actuator via the following series and parallel add-on components:

$$C_{2,s}(z^{-1}) = \frac{1}{1 - z^{-m_2} Q_2(z^{-1})} \tag{6}$$

$$C_{2,p}(z^{-1}) = \left[1 + \hat{P}_1(z^{-1}) C_1(z^{-1})\right] z^{-m_2} \hat{P}_2^{-1}(z^{-1}) Q_2(z^{-1}). \tag{7}$$

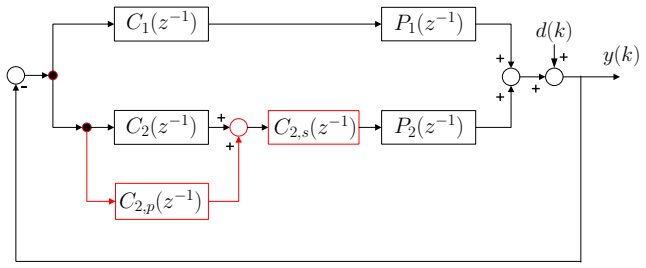

Figure 3: An equivalent block diagram of the system in Fig. 2: DDOB is decomposed to series and parallel modules.

3.1 Nominal Stability and Loop-shaping Criteria

From Fig. 3, the loop transfer function (obtained by cutting off the feedback line of $y(k)$) is

$$L = P_1 C_1 + P_2 C_{2,s}(C_2 + C_{2,p}) \tag{8}$$

$$= P_1 C_1 + P_2 \frac{C_2 + \left(1 + \hat{P}_1 C_1\right) z^{-m_2} \hat{P}_2^{-1} Q_2}{1 - z^{-m_2} Q_2}. \tag{9}$$

If $P_i = \hat{P}_i$, (9) simplifies to $L = \frac{P_1 C_1 + P_2 C_2 + z^{-m_2} Q_2}{1 - z^{-m_2} Q_2}$, and the sensitivity function of the closed-loop system is

$$S = \frac{1}{1+L} = \frac{1 - z^{-m_2} Q_2}{1 + P_1 C_1 + P_2 C_2}. \tag{10}$$

Notice that $1/(1 + P_1 C_1 + P_2 C_2)$ is the baseline closed-loop sensitivity function. S therefore is stable as long as Q_2 is stable. In addition, $1 - z^{-m_2} Q_2$ can be applied as a frequency-domain design criteria for the desired loop shaping. Specifically, from (10), the complementary sensitivity function is

$$T = 1 - S = \frac{P_1 C_1 + P_2 C_2 + z^{-m_2} Q_2}{1 + P_1 C_1 + P_2 C_2}. \tag{11}$$

In the frequency regions where $z^{-m_2} Q_2$ is approximately 1, $S \approx 0$ in (10) and $T \approx 1$ in (11), i.e., the closed-loop system has enhanced performance of disturbance rejection and reference following. When $z^{-m_2} Q_2$ is approximately 0, S and T are close to their baseline versions (without DDOB) and the original system response is preserved. One can remark that the proposed algorithm inherits the benefit of the SISO DOB [7] in that it uses a single filter Q_2 to flexibly enhance the system performance at the desired frequencies.

With slightly more algebra, we can obtain the closed-loop internal stability condition:

Theorem 1. *(nominal stability) Given an internally stable baseline feedback system, if the exact model of the plant is available; and $\hat{P}_2^{-1}(z^{-1})$ is stable, then the closed-loop system in Fig. 2 is internally stable as long as $Q_2(z^{-1})$ is stable.*

Proof. From (9), under the stated conditions, the closed-loop characteristic polynomial is given by

$$D_{Q_2} N_{\hat{P}_2} \times \left(D_{P_1} D_{P_2} D_{C_1} D_{C_2} + N_{P_1} N_{C_1} D_{P_2} D_{C_2} + N_{P_2} N_{C_2} D_{P_1} D_{C_1}\right)$$

where $N_{(\cdot)}$ and $D_{(\cdot)}$ denote respectively the numerator and denominator of a transfer function. Notice that $D_{P_1} D_{P_2} D_{C_1} D_{C_2} + N_{P_1} N_{C_1} D_{P_2} D_{C_2} + N_{P_2} N_{C_2} D_{P_1} D_{C_1}$ is the characteristic polynomial for the baseline system. The internal stability follows readily from the assumptions.

3.2 Robust Stability

Since plant uncertainty always exist in reality, actual implementation of the Q filter is constrained by the robust-stability condition. Consider the plant being perturbed to $\tilde{P}_i(e^{-j\omega}) = P_i(e^{-j\omega})\left(1 + W_i(e^{-j\omega})\Delta_i(e^{-j\omega})\right)$ $(i = 1, 2)$, where $W_i(e^{-j\omega})$'s are weighting functions, and the multiplicative disk uncertainties satisfy $\left\|\Delta_i(e^{-j\omega})\right\|_\infty \le 1$. Since the DISO system is a special multiple-input-multiple-output (MIMO) system, the μ-analysis (see, e.g., [17]) tool can be applied to derive the robust stability condition.

Theorem 2. *The closed-loop system in Fig. 2 is stable w.r.t. the perturbed plant if and only if the following structured singular value μ is strictly less than 1.*

$$\mu = \frac{|1 - z^{-m_2} Q_2||P_1 C_1||W_1|}{|1 + P_1 C_1 + P_2 C_2|} + \frac{|P_2 C_2 + (1 + P_1 C_1) z^{-m_2} Q_2||W_2|}{|1 + P_1 C_1 + P_2 C_2|}. \tag{12}$$

Proof. See Appendix B.

Remark: Overall (12) infers that in the regions where a good model is available for the plant (i.e., $|W_i|$ is small), the structured singular value is small and we have flexible design freedom in $Q_2(z^{-1})$. If $e^{-m_2 j\omega}Q_2(e^{-j\omega}) = 0$, DDOB is turned off at this frequency and (12) is simply the structured singular value of the baseline feedback system. This infers that the baseline system needs to be robustly stable. In the frequency region where $e^{-m_2 j\omega}Q_2(e^{-j\omega})$ is close to unity, $\mu \approx |W_2|$ and the robust stability depends on the model uncertainty of the secondary actuator. For dual-stage HDDs, accuracy of the model is usually preserved up to at least 5kHz, providing a large range for safe Q-filter design.

4 DESIGN OF Q FILTERS

From (10), forming $Q(z^{-1})$ as a low-pass filter yields the enhanced low-frequency servo performance similar to conventional SISO DOBs [7]. Various researches have been conducted w.r.t. designing such Q filters [18–20]. For vibration rejection, the disturbance is not restricted to occur at low frequencies. In this case, it is more beneficial to assign to $Q(z^{-1})$ a band-pass property. This section provides an optimal design of $Q(z^{-1})$ to achieve loop shaping at selective frequency locations. By using convex optimization techniques, we are able to design $Q(z^{-1})$ with arbitrary magnitude (upper) bounds and at the same time minimize the disturbance amplification in the closed-loop system.

Consider the following construction in (10):

$$1 - z^{-m}Q(z^{-1}) = F_{nf}(z^{-1})K(z^{-1}), \tag{13}$$

$$K(z^{-1}) = k_1 + k_2 z^{-1} + \ldots k_{n_k+1}z^{-n_k}. \tag{14}$$

Here $z^{-m}Q(z^{-1})$ can be either $z^{-m_1}Q_1(z^{-1})$ or $z^{-m_2}Q_2(z^{-1})$; $F_{nf}(z^{-1})$ is a notch filter that provides the desired low gains (in a range of frequencies) to (10) (see Fig. 6); $K(z^{-1})$ is essential for realizability of $Q(z^{-1})$ and provides additional optimal properties to $Q(z^{-1})$.

Consider the general notch-filter structure $F_{nf}(z^{-1}) = B_{nf}(z^{-1})/A_{nf}(z^{-1})$ with $B_{nf}(z^{-1}) = b_1 + b_2 z^{-1} + \cdots + b_{n_b+1}z^{-n_b}$ and $A_{nf}(z^{-1}) = a_1 + a_2 z^{-1} + \cdots + a_{n_a+1}z^{-n_a}$. Solving (13) gives

$$Q(z^{-1}) = z^m \frac{A_{nf}(z^{-1}) - B_{nf}(z^{-1})K(z^{-1})}{A_{nf}(z^{-1})} =: z^m \frac{X(z^{-1})}{A_{nf}(z^{-1})}.$$

Since z^m is not causal, to have a realizable $Q(z^{-1})$, the coefficients of z^{-i} $(i = 0, 1, \ldots, m-1)$ need to be zero in $X(z^{-1})$.[3] Expanding the convolution $B_{nf}(z^{-1})K(z^{-1})$ and grouping the coefficients in $A_{nf}(z^{-1}) - B_{nf}(z^{-1})K(z^{-1})$, we obtain the causality condition in the following matrix form:

$$\begin{bmatrix} a_1 \\ a_2 \\ \vdots \\ a_m \end{bmatrix} - \begin{bmatrix} b_1 & 0 & 0 & 0 & 0_{1,n_k+1-m} \\ b_2 & b_1 & 0 & 0 & 0_{1,n_k+1-m} \\ \vdots & \ddots & \ddots & 0 & 0_{1,n_k+1-m} \\ b_m & \ldots & b_2 & b_1 & 0_{1,n_k+1-m} \end{bmatrix} \begin{bmatrix} k_1 \\ k_2 \\ \vdots \\ \vdots \\ k_{n_k+1} \end{bmatrix} = 0. \tag{15}$$

If $n_k + 1 = m$, the m equations in (15) define a unique solution for $K(z^{-1})$. Additionally, n_k can be set to be larger than $m-1$ so as to allow more design freedom in $Q(z^{-1})$. First, we can minimize the infinity norm of $1 - z^{-m}Q(z^{-1})$ (maximum magnitude in frequency response), which will in turn minimize the disturbance amplification in the sensitivity function (10). This can be achieved by minimizing $\|K(z^{-1})\|_\infty$ in (13). Second, as discussed in Section 3.2, to keep the system robustly stable, the magnitude of $Q(z^{-1})$ should be small at frequencies outside its passband, especially at the frequencies where large model uncertainty exists (normally in the high-frequency region). This corresponds to confining $|Q(e^{-j\omega_i})| \le \epsilon_i$, where ϵ_i is some user-defined bound and ω_i is the frequency at which the magnitude constraint is required (there can be multiple of such constraints).

By applying the bounded-real lemma, the H_∞-performance objective (i.e., $\min\|K(z^{-1})\|_\infty$) can be translated to a linear matrix inequality (LMI) [21, 22]. The causality constraint (15) is a set of linear equations.[4] In addition, due to the FIR construction of $K(z^{-1})$ in (13), the gain constraint $|Q(e^{-j\omega_i})| \le \epsilon_i$ can be transformed to a convex quadratic constraint. To see this point, notice first that $|Q(e^{-j\omega_i})| \le \epsilon_i$ is equivalent to $|Q(e^{-j\omega_i})|^2 \le \epsilon_i^2$. Denoting $\theta = [\,k_1, k_2, \ldots\, k_{n_k+1}\,]^T$ as the coefficient vector of $K(z^{-1})$ in (13-14), we can express the inequality $|Q(e^{-j\omega_i})|^2 = \left|z^m(1 - F_{nf}(z^{-1})K(z^{-1}))\right|_{z=e^{j\omega_i}}\right|^2 \le \epsilon_i^2$ in the following quadratic form of θ:

$$\theta^T\left[\psi_r(\omega_i)\psi_r^T(\omega_i) + \psi_m(\omega_i)\psi_m^T(\omega_i)\right]\theta - 2\psi_r^T(\omega_i)\theta + 1 \le \epsilon_i^2 \tag{16}$$

[3] If $m = 0$, causality is automatically satisfied.

[4] Explicitly $n_k > m-1$ is assumed in this case, since if $n_k = m-1$ then the solution of $K(z^{-1})$ is unique from (15).

with

$$\psi_r^T(\omega_i) = F_r(\omega_i)\phi_r^T(\omega_i) - F_m(\omega_i)\phi_m^T(\omega_i)$$
$$\psi_m^T(\omega_i) = F_r(\omega_i)\phi_m^T(\omega_i) + F_m(\omega_i)\phi_r^T(\omega_i)$$
$$F_{nf}(e^{-j\omega_i}) = F_r(\omega_i) - jF_m(\omega_i)$$
$$\phi_r^T(\omega_i) = \left[1, \cos(\omega_i), \ldots \cos(n_k\omega_i)\right]$$
$$\phi_m^T(\omega_i) = \left[0, \sin(\omega_i), \ldots \sin(n_k\omega_i)\right].$$

Here $\phi_r(\omega_i)$ and $\phi_m(\omega_i)$ come from coefficients of the real and the imaginary parts of $K(e^{-j\omega_i}) \triangleq \phi_r^T(\omega_i)\theta - j\phi_m^T(\omega_i)\theta$; $\psi_r(\omega_i)$ and $\psi_m(\omega_i)$ are from $F_{nf}(e^{-j\omega_i})K(e^{-j\omega_i}) \triangleq \psi_r^T(\omega_i)\theta - j\psi_m^T(\omega_i)\theta$; and (16) is obtained by substituting $F_{nf}(e^{-j\omega_i})K(e^{-j\omega_i})$ into $|Q(e^{-j\omega_i})|^2 = |1 - F_{nf}(e^{-j\omega_i})K(e^{-j\omega_i})|^2$.

Notice that (16) is a convex constraint in θ, since $\psi_r(\omega_i)\psi_r^T(\omega_i) + \psi_m(\omega_i)\psi_m^T(\omega_i)$ is positive semi-definite.

Summarizing the above discussions, we obtain the following constrained optimization problem

$$\min_{\theta,P,\gamma} : \gamma$$
$$\text{s.t.: causality constraint} \tag{17}$$
$$\begin{bmatrix} A^TPA - P & A^TPB & C^T \\ B^TPA & B^TPB - \gamma I & D^T \\ C & D & -\gamma I \end{bmatrix} \le 0,\ P > 0 \tag{18}$$
$$\theta^T\left[\psi_r(\omega_i)\psi_r^T(\omega_i) + \psi_m(\omega_i)\psi_m^T(\omega_i)\right]\theta - 2\psi_r^T(\omega_i)\theta + 1 \le \epsilon_i^2,\ i = 1,2,\ldots \tag{19}$$

where 's.t.' denotes 'subject to' and we have translated the objective of 'min : $\|K(z^{-1})\|_\infty$' to 'min : γ s.t. (18)' (using the bounded-real lemma). Here A, B, C and D are the state-space matrices of $K(z^{-1})$. We choose the controllable canonical form

$$A = \begin{bmatrix} 0_{n_k-1,1} & I_{n_k-1} \\ 0 & 0_{1,n_k-1} \end{bmatrix},\ B = \begin{bmatrix} 0_{n_k-1,1} \\ 1 \end{bmatrix}$$
$$C = \left[k_2, \ldots, k_{n_k+1}\right],\quad D = k_1$$

such that (18) is linear in the decision variables θ and P. The entire optimization problem is now convex, and can be efficiently solved using the interior-point method (see, e.g., [23]) in modern optimization.

5 CASE STUDY

The proposed DDOBs are applied in this section to a simulated example that uses the system configuration on page 195 of the book [24]. The plant model comes from identification of an actual experimental setup. A set of disturbance data is obtained from audio-vibration tests on an actual HDD. The top plot of Fig. 7 shows the resulting spectrum of the position error signal, where it is observed that large spectral peaks appear at 1000 Hz and 3000 Hz. We will design DDOBs for both the Voice-Coil-Motor (VCM) and microactuator (MA) actuators. The former is denoted as VCM DDOB, and the latter as MA DDOB.

Two major resonances exist in the VCM plant, and are compensated via two notch filters at 3.0 kHz and 6.5 kHz. The 11-order resonance-compensated VCM model is treated as a generalized plant $P_1(z^{-1})$. Such a design enables a reduced-order and minimum-phase $\hat{P}_1(z^{-1})$. As the notch filters introduced some additional phase loss to $P_1(z^{-1})$, overall $\hat{P}_1(z^{-1})$ contains a 2-step delay, i.e., $m_1 = 2$. After the above construction, one non-minimum-phase zero appears in $\hat{P}_1(z^{-1})$ near the Nyquist frequency. This zero is replaced with a stable one that lies strictly inside the unit circle, yielding the final nominal model shown in Fig. 4. Through the above design, both the magnitude and the phase of $P_1(z^{-1})$ is well captured by $\hat{P}_1(z^{-1})$ up to around 6 kHz.

The microactuator also contains two resonances that are compensated by notch filters (at 6.5 kHz and 9.6 kHz). This actuator is a minimum-phase system (DC gain plus resonances) by nature, which simplifies the $\hat{P}_2(z^{-1})$ design. We directly model $\hat{P}_2(z^{-1})$ to include the resonances and have $m_2 = 1$ in Fig. 1.

The decoupled sensitivity design (see, e.g., [4]) is used to form the baseline feedback loop. The baseline closed-loop sensitivity function has the magnitude response shown by the solid line in Fig. 5. We can recognize that such a loop shape is quite standard in feedback control.

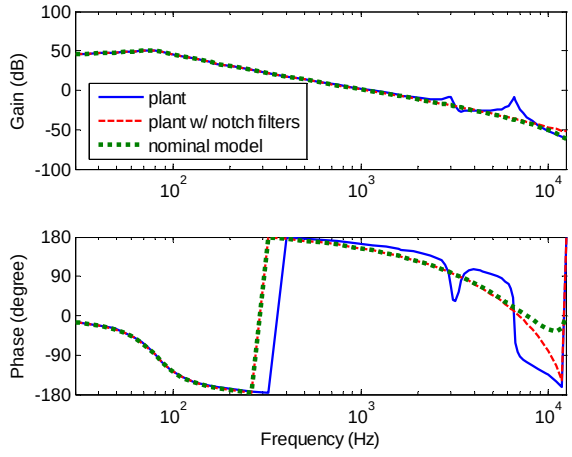

Figure 4: $\hat{P}_1(z^{-1})$ design for DDOB in VCM actuation stage.

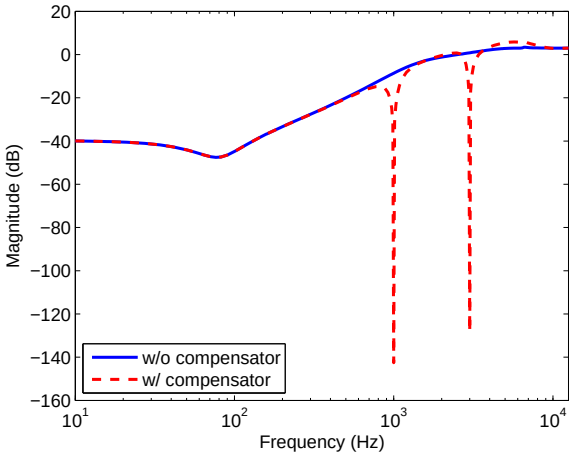

Figure 5: Magnitude responses of the sensitivity functions with and without DDOBs.

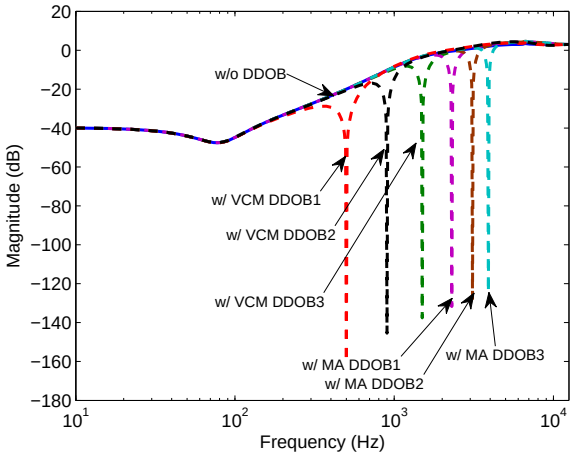

Figure 6: Magnitude responses of the sensitivity functions with different Q-filter configurations.

VCM DDOB is configured to work at the low-frequency region, with a band-pass Q filter that is centered at 1000 Hz with a passband of 400 Hz. MA DDOB aims at rejecting the high-frequency disturbances, with a 600 Hz-passband band-pass Q filter centering at 3000 Hz. From the resulting magnitude response of the sensitivity function (the dashed line in Fig. 5), it is observed that two deep notches are created at the corresponding Q-filter center frequencies, indicating the strong disturbance rejections there. In the Q-filter design, we have constructed $F_{nf}(z^{-1}) = \frac{1-2\cos\omega_0 z^{-1}+z^{-2}}{1-2\alpha\cos\omega_0 z^{-1}+\alpha^2 z^{-2}}$ in (13), and constrained the optimal $Q(z^{-1})$ to have its gains at DC and Nyquist frequency to be lower than -50dB. This contributes to the strongly retained baseline loop shape in Fig. 5. Due to Bode's Integral Theorem, some magnitude increase occurs around 5 kHz. Such amplification can be reduced by designing the notch filter $F_{nf}(z^{-1})$ to be not as sharp as presented.

The flexibility of DDOB is explained in Fig. 6, where we fix z^{-m_i} and $\hat{P}_i(z^{-1})$ in DDOBs and vary the center frequency of the Q filter. Six Q filters are evaluated, with the resulting six sensitivity functions plotted in an overlaid fashion. The first three gain reductions come from VCM DDOB with $Q_1(z^{-1})$ centered at 500 Hz, 900 Hz, and 1500 Hz respectively. The remaining three are generated by MA DDOB ($Q_2(z^{-1})$ centered at 2300 Hz, 3100 Hz, and 3900 Hz). It is observed that by simple alternation of Q filters, the servo loop can be customized to a great extension.

Figs. 7 and 8 present respectively the frequency- and time-domain servo performances using a modified version of the disturbance data from actual vibration tests. It can be observed that the spectral peaks at the corresponding frequencies are significantly reduced by DDOBs, and that the magnitudes of position errors are decreased to be less than one half of the original values.

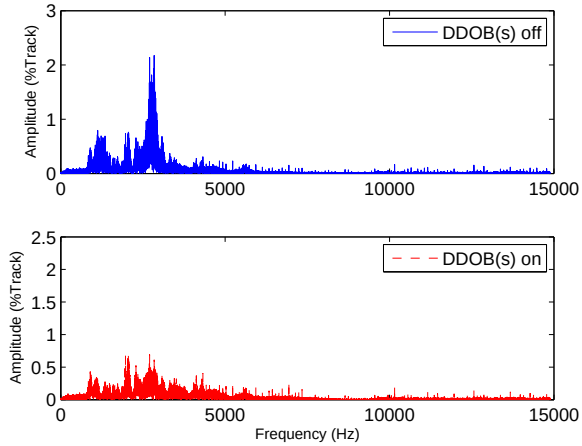

Figure 7: Spectra of the position error signals using a projected disturbance profile from actual experiments.

6 CONCLUSIONS

This paper has presented a flexible feedback control approach for servo enhancement in dual-input-single-output control systems. Specifically we have discussed the application of the algorithm to compensate disturbances in dual-stage hard disk drives. The advantages of decoupled disturbance rejection, extended high-frequency disturbance rejection in HDD systems, and optimal Q-filter design, have been discussed in details.

ACKNOWLEDGMENT

This work was supported in part by the Computer Mechanics Laboratory (CML) in the Department of Mechanical Engineering, University of California, Berkeley and by

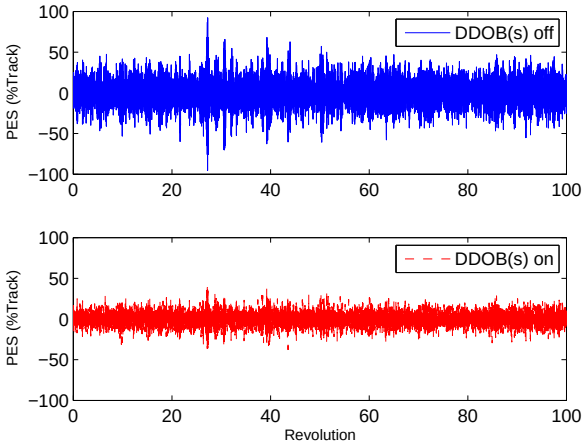

Figure 8: Time traces of the position error signals in Fig. 7.

a research grant from Western Digital Corporation.

References

[1] Abramovitch, D. Y., and Franklin, G. F., 2002. "A brief history of disk drive control". *IEEE Control Syst. Mag.*, **22**(3), pp. 28–42.

[2] Al Mamun, A., and Ge, S. S., 2005. "Precision control of hard disk drives". *IEEE Control Syst. Mag.*, **25**(4), pp. 14–19.

[3] Suthasun, T., Mareels, I., and Al Mamun, A., 2004. "System identification and controller design for dual actuated hard disk drive". *Control Engineering Practice*, **12**(6), pp. 665–676.

[4] Horowitz, R., Li, Y., Oldham, K., Kon, S., and Huang, X., 2007. "Dual-stage servo systems and vibration compensation in computer hard disk drives". *Control Engineering Practice*, **15**(3), pp. 291–305.

[5] White, M., Tomizuka, M., and Smith, C., 2000. "Improved track following in magnetic disk drives using a disturbance observer". *IEEE/ASME Trans. Mechatronics*, **5**(1), Mar., pp. 3–11.

[6] Jia, Q.-W., 2009. "Disturbance rejection through disturbance observer with adaptive frequency estimation". *IEEE Trans. Magn.*, **45**(6), June, pp. 2675–2678.

[7] Ohnishi, K., 1993. "Robust motion control by disturbance observer". *Journal of the Robotics Society of Japan*, **11**(4), pp. 486–493.

[8] Yang, K., Choi, Y., and Chung, W. K., 2005. "On the tracking performance improvement of optical disk drive servo systems using error-based disturbance observer". *IEEE Trans. Ind. Electron.*, **52**(1), Feb., pp. 270–279.

[9] Tan, K. K., Lee, T. H., Dou, H. F., Chin, S. J., and Zhao, S., 2003. "Precision motion control with disturbance observer for pulsewidth-modulated-driven permanent-magnet linear motors". *IEEE Trans. Magn.*, **39**(3), pp. 1813–1818.

[10] Kempf, C. J., and Kobayashi, S., 1999. "Disturbance observer and feedforward design for a high-speed direct-drive positioning table". *IEEE Trans. Control Syst. Technol.*, **7**(5), pp. 513–526.

[11] Eom, K. S., Suh, I. H., and Chung, W. K., 2001. "Disturbance observer based path tracking control of robot manipulator considering torque saturation". *Mechatronics*, **11**(3), pp. 325 – 343.

[12] Bohn, C., Cortabarria, A andHärtel, V., and Kowalczyk, K., 2004. "Active control of engine-induced vibrations in automotive vehicles using disturbance observer gain scheduling". *Control Engineering Practice*, **12**(8), pp. 1029 – 1039.

[13] Nie, J., and Horowitz, R., 2009. "Design and implementation of dual-stage track-following control for hard disk drives". In Proc. 2nd Dynamic Systems and Control Conf., Vol. 2, pp. 565–572.

[14] Guo, L., and Chen, W.-H., 2005. "Disturbance attenuation and rejection for systems with nonlinearity via dobc approach". *International Journal of Robust and Nonlinear Control*, **15**(3), pp. 109–125.

[15] Zheng, Q., Chen, Z., and Gao, Z., 2009. "A practical approach to disturbance decoupling control". *Control Engineering Practice*, **17**(9), pp. 1016–1025.

[16] Deller, J. R., Hansen, J. H. L., and Proakis, J. G., 1999. *Discrete-Time Processing of Speech Signals*. Wiley-IEEE Press, Sept.

[17] Zhou, K., and Doyle, J. C., 1998. *Essentials of robust control*. Prentice Hall New Jersey, Oct.

[18] Wang, C.-C., and Tomizuka, M., 2004. "Design of robustly stable disturbance observers based on closed loop consideration using h-infinity optimization and its applications to motion control systems". In Proc. 2004 American Control Conf., Vol. 4, pp. 3764 –3769.

[19] Kemp, C. C., and Kobayashi, S., 1996. "Discrete-time disturbance observer design for systems with time delay". In Proc. 1996 4th International Workshop on Advanced Motion Control, Vol. 1, pp. 332–337.

[20] Choi, Y., Yang, K., Chung, W. K., Kim, H. R., and Suh, I. H., 2003. "On the robustness and performance of disturbance observers for second-order systems". *IEEE Trans. Autom. Control*, **48**(2), Feb., pp. 315–320.

[21] Scherer, C., Gahinet, P., and Chilali, M., 1997. "Multiobjective output-feedback control via LMI optimization". *IEEE Trans. Autom. Control*, **42**(7), July, pp. 896–911.

[22] Boyd, S. P., El Ghaoui, L., Feron, E., and Balakrishnan, V., 1994. *Linear matrix inequalities in system and control theory*. Society for Industrial Mathematics.

[23] Grant, M., and Boyd, S., 2011. CVX: Matlab software for disciplined convex programming, version 1.21. http://cvxr.com/cvx, Feb.

[24] Al Mamun, A., Guo, G., and Bi, C., 2007. *Hard disk drive: mechatronics and control*. CRC Press.

Appendix A: Equivalence between Figs. 2 and 3:

In Fig. 2, splitting the output of $Q_2(z^{-1})$ into two parts, and relocating the summing junction after $\hat{P}_1(z^{-1})$, we get Fig. 9a. Since the reference is zero, Fig. 9a is equivalent to Fig. 9b. Finally noting that the $\hat{P}_1(z^{-1})C_1(z^{-1})$ block in Fig. 9b does not influence the path from $C_1(z^{-1})$ to $P_1(z^{-1})$, we obtain Fig. 3, the equivalent block diagram for analysis, with the add-on serial and parallel terms given by (6) and (7).

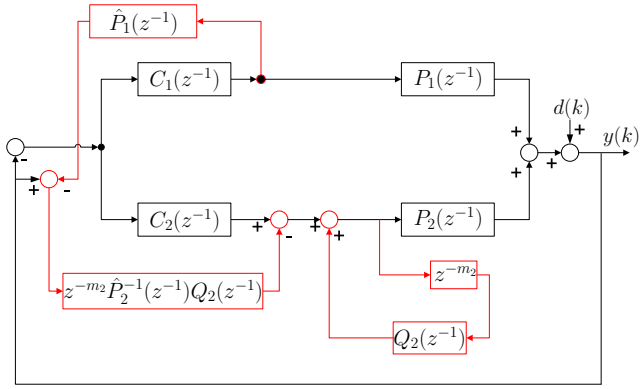

(a) An equivalent block diagram of the system in Fig. 2: the input to $z^{-m_2}\hat{P}_2(z^{-1})$ is relocated; the summing junction before $Q_2(z^{-1})$ is separated.

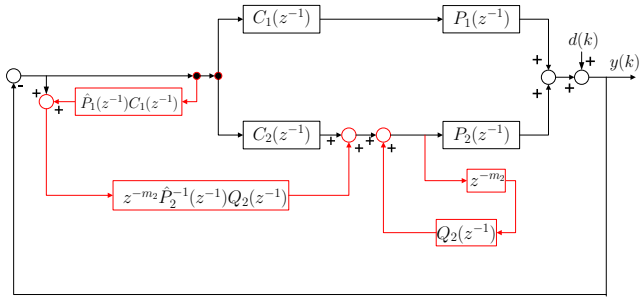

(b) An equivalent block diagram of the system in Fig. 3: the signs of the signals are changed, after another relocation of block diagrams.

Figure 9: Block diagram transformation for Fig. 2.

Appendix B: Proof of Theorem 2

Consider first the general closed-loop system for DISO plants under perturbation, as shown in Fig. 10, wherein $\tilde{C}_i$'s are the equivalent feedback controller. To obtain the robust stability condition, we first transform Fig. 10 to the generalized representation in Fig. 11.

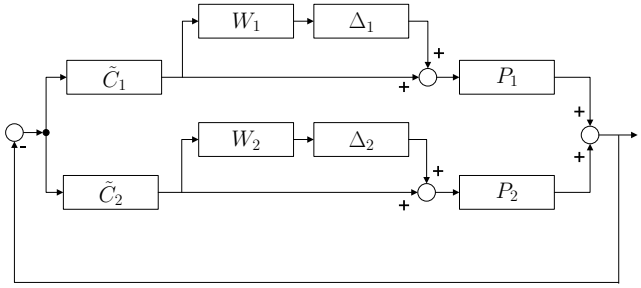

Figure 10: The general closed-loop system for DISO plants under perturbations.

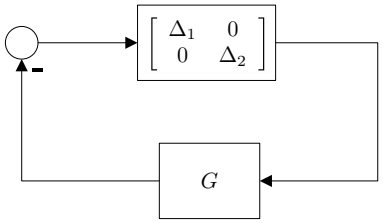

Figure 11: The generalized block diagram of Fig. 10

From μ-analysis, the closed-loop system is stable w.r.t. the plant perturbations if and only if G is stable and the structured singular value of G satisfies: $\forall\omega$, $\mu_\Delta\left(G(e^{-j\omega})\right)<1$. In Fig. 11, consider the smallest (in the sense of H_∞ norm) perturbation Δ such that the following stability boundary is attained:

$$\det\left(I+\Delta(e^{-j\omega})G(e^{-j\omega})\right)=0. \tag{20}$$

After standard block-diagram analysis, the generalized plant G can be shown to be

$$G=\frac{W\tilde{C}P}{1+P\tilde{C}}=\frac{1}{1+P_1\tilde{C}_1+P_2\tilde{C}_2}\begin{bmatrix}W_1\tilde{C}_1\\ W_2\tilde{C}_2\end{bmatrix}\begin{bmatrix}P_1 & P_2\end{bmatrix}. \tag{21}$$

Substituting $\Delta=diag\{\Delta_1,\Delta_2\}$ and (21) to (20) yields (for simplified notation, the frequency index $e^{-j\omega}$ is omitted)

$$\begin{aligned}&\det(I+\Delta G)\\ =&\det\left(I+\frac{\begin{bmatrix}\Delta_1 & 0\\ 0 & \Delta_2\end{bmatrix}}{1+P_1\tilde{C}_1+P_2\tilde{C}_2}\begin{bmatrix}W_1\tilde{C}_1\\ W_2\tilde{C}_2\end{bmatrix}\begin{bmatrix}P_1 & P_2\end{bmatrix}\right)\\ =&1+\frac{P_1\Delta_1W_1\tilde{C}_1+P_2\Delta_2W_2\tilde{C}_2}{1+P_1\tilde{C}_1+P_2\tilde{C}_2},\end{aligned} \tag{22}$$

where the last equality used the determinant identity $\det(I+AB)=\det(I+BA)$.

Combining (22) and (20), the minimum-H_∞-norm perturbation is obtained if $|\Delta_1| = |\Delta_2| =: |\Delta_0|$ and the following equality holds

$$1 - \left|\frac{P_1 W_1 \tilde{C}_1}{1 + P_1\tilde{C}_1 + P_2\tilde{C}_2}\right||\Delta_0| - \left|\frac{P_2 W_2 \tilde{C}_2}{1 + P_1\tilde{C}_1 + P_2\tilde{C}_2}\right||\Delta_0| = 0.$$

By definition (see, e.g., [17]), the structured singular value is

$$\mu = \frac{1}{|\Delta_0|} = \frac{\left|P_1\tilde{C}_1\right||W_1| + \left|P_2\tilde{C}_2\right||W_2|}{\left|1 + P_1\tilde{C}_1 + P_2\tilde{C}_2\right|}. \tag{23}$$

When DDOB is in the feedback loop as shown in Fig. 3, $\tilde{C}_1 = C_1$ and $\tilde{C}_2 = C_{2,s}\left(C_2 + C_{2,p}\right)$, where $C_{2,s}$ and $C_{2,p}$ are given by (6) and (7). Therefore, assuming $\hat{P}_i = P_i$, after simplification, one can get the explicit form of (12).